Nonlinear silicon-on-insulator waveguides for all-optical signal processing

C. Koos, L. Jacome, C. Poulton, J. Leuthold and W. Freude

Institute of High-Frequency and Quantum Electronics, University of Karlsruhe, 76131 Karlsruhe, Germany

C.Koos@ihq.uka.de, W.Freude@ihq.uka.de

http://www.ihq.uni-karlsruhe.de

Abstract: Values up to $\gamma = 7 \times 10^6/(\mathrm{W\,km})$ for the nonlinear parameter are feasible if silicon-on-insulator based strip and slot waveguides are properly designed. This is more than three orders of magnitude larger than for state-of-the-art highly nonlinear fibers, and it enables ultrafast all-optical signal processing with nonresonant compact devices. At $\lambda = 1.55\,\mu$m we provide universal design curves for strip and slot waveguides which are covered with different linear and nonlinear materials, and we calculate the resulting maximum γ.

OCIS codes: (130.4310) Nonlinear; (130.2790) Guided Waves; (160.4330) Nonlinear optical materials; (190.3270) Kerr effect; (190.4710) Optical nonlinearities in organic materials; (190.5970) Semiconductor nonlinear optics.

References and links

1. B. E. Little, J. S. Foresi, G. Steinmeyer, E. R. Toen, S. T. Chu, H. A. Haus, E. P. Ippen, L. C. Kimerling, and W. Greene. "Ultra-compact Si–SiO_2 microring resonator optical channel dropping filters," IEEE Photon. Technol. Lett. 10:549–551, 1998.
2. T. Fukazawa, F. Ohno, and T. Baba. "Very compact arrayed waveguide grating using Si photonic wire waveguides," Japan. Journ. of Appl. Phys. 43:L673–L675, 2004.
3. W. Bogaerts, R. Baets, P. Dumon, V. Wiaux, S. Beckx, D. Taillaert, B. Luyssaert, J. Van Campenhout, P. Bienstmann, and D. Van Thourhout. "Nanophotonic waveguides in silicon-on-insulator fabricated with CMOS technology," J. Lightw. Technol. 23:401–412, 2005.
4. T. Tsuchizawa, K. Yamada, H. Fukuda, T. Watanabe, J. Takahashi, M. Takahashi, T. Shoji, E. Tamechika, S. Itabashi, and H. Morita. "Microphotonics devices based on silicon microfabrication technology," IEEE J. Sel. Topics Quantum Electron. 11(1):232, 2005.
5. Y. A. Vlasov, M. O'Bolye, H. F. Hamann, and S. J. McNab. "Active control of slow light on a chip with photonic crystal waveguides," Nature 438:65–69, November 2005.
6. M. Lipson. "Guiding, modulating, and emitting light on silicon — challenges and opportunities," J. Lightw. Technol. 23:4222–4238, 2005.
7. C. A. Barrios. "High-performance all-optical silicon microswitch," Electron. Lett. 40, 2004.
8. T. Fujisawa and M. Koshiba. "All-optical logic gates based on nonlinear slot-waveguide couplers," J. Opt. Soc. Am. B 23:684–691, 2006.
9. H. K. Tsang, C. S. Wong, T. K. Liang, I. E. Day, S. W. Roberts, A. Harpin, J. Drake, and M. Asghari. "Optical dispersion, two-photon absorption and self-phase modulation in silicon waveguides at 1.5μm wavelength," Appl. Phys. Lett. 80:416–418, 2002.
10. H. Yamada, M. Shirane, T. Chu, H. Yokoyama, S. Ishida, and Y. Arakawa. "Nonlinear-optic silicon-nanowire waveguides," Japan. Journ. of Appl. Phys. 44:6541–6545, 2005.
11. E. Dulkeith, Y. A. Vlasov, X. Chen, N. C. Panoiu, and R. M. Osgood. "Self-phase-modulation in submicron silicon-on-insulator photonic wires," Opt. Express 14:5524–5534, 2006.
12. V. R. Almeida, Q. Xu, C. A. Barrios, and M. Lipson. "Guiding and confining light in void nanostructure," Opt. Lett. 29:1209, 2004.

#81030 - $15.00 USD Received 14 Mar 2007; revised 25 Apr 2007; accepted 27 Apr 2007; published 1 May 2007

13. Q. Xu, V. R. Almeida, R. R. Panepucci, and M. Lipson. "Experimental demonstration of guiding and confining light in nanometer-size low-refractive-index material," Opt. Lett. 29:1626, 2004.
14. P. Müllner and R. Hainberger. "Structural optimization of silicon-on-insulator slot waveguides," IEEE Photon. Technol. Lett. 18:2557–2559, 2006.
15. G. P. Agrawal. Nonlinear Fiber Optics. Academic Press, San Diego, third edition, 2001.
16. J. Y. Y. Leong, P. Petropoulos, S. Asimakis, H. Ebendorff-Heideprim, R. C. Moore, Ken. Frampton, V. Finazzi, X. Feng, J. H. V. Price, T. M. Monro, and D. J. Richardson. "A lead silicate holey fiber with $\gamma = 1860(\mathrm{Wkm})^{-1}$ at 1550nm," In Optical Fiber Communication (OFC) Conference Anaheim (CA), USA, March 2005. PDP22.
17. Y. R. Shen. Nonlinear Optics. John Wiley and Sons, New York, 1984.
18. X. Chen, N. C. Panoiu, and R. M. Osgood. "Theory of raman-mediated pulsed amplification in silicon-wire waveguides," IEEE J. Quantum Electron. 42:160–170, 2006.
19. RSoft Design Group, Inc., http://www.rsoftdesign.com. FemSIM 2.0 User Guide 2005.
20. J. J. Wynne. "Optical third-order mixing in GaAs, Ge, Si and InAs," Phys. Rev. 178:1295–1301, February 1969.
21. H. Fukuda, K. Yamada, T. Shoji, M. Takahashi, T. Tsuchizawa, T. Watanabe, J. Takahasi, and S. Itabashi. "Four-wave mixing in silicon wire waveguides," Opt. Express 13:4629–4637, 2005.
22. V. Mizrahi, K. W. DeLong, G. I. Stegeman, M. A. Saifi, and M. J. Andrejco. "Two-photon absorption as a limitation to all-optical switching," Opt. Lett. 14:1140–1142, December 1989.
23. U. Gubler and C. Bosshard. Molecular design for third-order nonlinear optics. Advances in Polymer Science 158:123–191, 2002.
24. M. Dinu, F. Quochi, and H. Garcia. "Third-order nonlinearities in silicon at telecom wavelengths," Appl. Phys. Lett. 82:2954–2956, 2003.
25. R. S. Friberg and P. W. Smith. "Nonlinear optical glasses for ultrafast optical switches," IEEE J. Quantum Electron. 23:2089, 1987.
26. K. Kikuchi, K. Taira, and N. Sugimoto. "Highly nonlinear bismuth oxide-based glass fibers for all-optical signal processing," Electron. Lett. 38:166, 2002.
27. H. Nasu, O. Matsushita, K. Kamiya, H. Kobayashi, and K. Kubodera. "Third harmonic generation from Li_2O–TiO_2–TeO_2 glasses," J. Non-Cryst. Solids. 124:275–277, 1990.
28. T. Cardinal, K. A. Richardson, H. Shim, A. Schulte, R. Beatty, K. Le Foulgoc, C. Meneghini, J. F. Viens, and A. Villeneuve. "Non-linear optical properties of chalcogenide glasses in the system As–S–Se," J. Non-Cryst. Solids. 256&257:353–360, 1999.
29. J. M. Harbold, F. Ö. Ilday, F. W. Wise, J. S. Sanghera, V. Q. Nguyen, L. B. Shaw, and I. D. Aggarwal. "Higly nonlinear As-S-Se glasses for all-optical switching," Opt. Lett. 27:119–121, 2002.
30. P. D. Townsend, G. L. Baker, N. E. Schlotter, C. F. Klausner, and S. Eternad. "Waveguiding in spun films of soluble polydiacetylenes," Appl. Phys. Lett. 53:1782–1784, 1988.
31. K. Rochford, R. Zanoni, G. I. Stegeman, W. Krug, E. Miao, and M. W. Beranek. "Measurement of nonlinear refractive index and transmission in polydiacetlyene waveguides at 1.319μm," Appl. Phys. Lett. 58:13–15, 1991.
32. U. Gubler. Third-order nonlinear optical effects in organic materials. PhD thesis, Swiss Federal Institute of Technology Zürich, 2000.
33. T. Kaino. "Waveguide fabrication using organic nonlinear optical materials," J. Opt. A: Pure Appl. Opt. 2:R1–R7, 2000.
34. M. Asobe, I. Yokohama, T. Kaino, S. Tomaru, and T. Kurihara. Nonlinear absorption and refraction in an organic dye functionalized main chain polymer waveguide in the 1.5μm wavelength region. Appl. Phys. Lett. 67:891–893, 1995.
35. D. Y. Kim, M. Sundheimer, A. Otomo, G. Stegeman, W. H. G. Horsthuis, and G. R. Möhlmann. "Third order nonlinearity of 4-dialkyamino-4'nitro-stilbene waveguides at 1319nm," Appl. Phys. Lett. 63:290–292, 1993.
36. A. K. Bhowmik and M. Thakur. "Self-phase modulation in polydiacetylene single crystal measured at 720-1064nm," Opt. Lett. 26:902–904, 2000.
37. B. L. Lawrence, M. Cha, J. U. Kang, W. Toruellas, G. Stegemann, G. Baker, J. Meth, and S. Etemad. "Large purely refractive nonlinear index of single-crystal P-toluene sulphonate (PTS) at 1600nm," Electron. Lett. 30:447–448, 1994.
38. G. Vijaya Prakash, M. Cazzanelli, Z. Gaburro, L. Pavesi, F. Iacona, G. Franzo, and F. Priolo. "Linear and nonlinear optical properties of plasma-enhanced chemical-vapour deposition grown silicon nanocrystals," J. Mod. Opt. 49:719–730, 2002.
39. T. Fujisawa and M. Koshiba. "Guided modes of nonlinear slot waveguides," IEEE Photon. Technol. Lett. 18:1530–1532, 2006.
40. D. Marcuse. Light Transmission Optics. Van Nostrand Reinhold, New York, 1972.

1. Introduction

Silicon-on-insulator (SOI) is considered a promising material system for dense on-chip integration of both photonic and electronic devices. Providing low absorption at infrared telecom-

#81030 - $15.00 USD Received 14 Mar 2007; revised 25 Apr 2007; accepted 27 Apr 2007; published 1 May 2007

munication wavelengths and having a high refractive index of $n \approx 3.48$, silicon is well suited for building compact linear optical devices [1–6]. To efficiently use their inherently large optical bandwidth, it is desirable to perform all-optical signal processing and switching on the same chip by exploiting ultrafast $\chi^{(3)}$-nonlinearities such as four-wave-mixing (FWM), cross- and self-phase modulation (XPM, SPM) or two-photon absorption (TPA). Such devices show potential for ultrafast all-optical switching at low power [7, 8].

Third-order nonlinear interaction in SOI-based waveguides can be realized in two ways: First, nonlinear interaction with the silicon waveguide core itself can be used, leading to SPM/XPM overlayed by TPA [9–11]. Second, the silicon core can be embedded in nonlinear cladding material, and interaction with the evanescent part of the guided mode can be exploited. In the latter case, interaction with the nonlinear cladding material can be significantly enhanced when using slot waveguides rather than strips [12, 13], whereby the fraction of optical power guided in the low-index region can be maximized by appropriate waveguide dimensions [14].

However, it is not clear from the beginning, which choice leads to more pronounced nonlinearities. The strength of third-order nonlinear interaction in a waveguide is described by the nonlinear parameter γ, the real part of which depends on the waveguide geometry as well as on the nonlinear-index coefficient n_2 of the nonlinear interaction material. To optimize the waveguide dimensions for maximal nonlinear interaction, a geometrical measure is needed to rate the spatial confinement of the mode inside the nonlinear material. For optical fibers or other low index-contrast waveguides, the light propagates inside a quasi-homogeneous nonlinear material, and an appropriate measure is the so-called effective core area for nonlinear interaction A_{eff} [15] which is calculated based on a scalar approximation of the modal field. The actual cross-sectional power P related to the effective core area A_{eff} accounts then for the nonlinear deviation $n_2 P/A_{\text{eff}}$ from the linear effective refractive index of the waveguide mode.

This widely used notion of an effective area cannot be directly transferred to nonlinear high index-contrast SOI waveguides. In addition, the nonlinearity is usually limited to certain subdomains of the modal cross section.

In this paper we therefore first extend the standard definition of A_{eff} to the case of a high index-contrast $\chi^{(3)}$-nonlinear waveguide and calculate its effective area A_{eff}. The smaller A_{eff} becomes, the larger the nonlinear effects will be for a given $\chi^{(3)}$. We then calculate universal design parameters for a silicon core and for various cover materials leading to a minimum A_{eff} for strip and slot waveguides at the telecommunication wavelength $\lambda = 1.55\,\mu$m. We estimate the nonlinear waveguide parameter γ for optimized waveguide geometries. We find that γ can become more than three orders of magnitude larger ($\sim 7 \times 10^6/(\text{W km})$) than for state-of-the-art highly nonlinear fibers ($\sim 2 \times 10^3/(\text{W km})$ [16]), and we infer that ultrafast all-optical switching is feasible with non-resonant mm-scale SOI-based devices.

The paper is structured as follows: In Section 2, we define the effective area A_{eff} for nonlinear interaction in high index-contrast waveguides; mathematical details are given in the Appendix. In Section 3, we describe the waveguide optimization method, and in Section 4 we present optimal parameters for different types of SOI-based waveguides. Section 5 deals with different interaction materials; we calculate γ for various waveguides, and we discuss application examples. Section 6 summarizes the work.

2. Effective area for third-order nonlinear interaction

Figure 1 shows cross sections of the waveguides under consideration. The core domain D_{core} consists of silicon ($n_{\text{core}} \approx 3.48$ for $\lambda = 1.55\,\mu$m), the substrate domain D_{sub} is made out of silica ($n_{\text{sub}} \approx 1.44$), and the cover domain D_{cover} comprises a cladding material with refractive index $n_{\text{cover}} < n_{\text{core}}$. For the strip waveguide in Fig. 1(a), nonlinear interaction can either occur within the waveguide core ("core nonlinearity"), or the evanescent part of the guided light

#81030 - $15.00 USD Received 14 Mar 2007; revised 25 Apr 2007; accepted 27 Apr 2007; published 1 May 2007

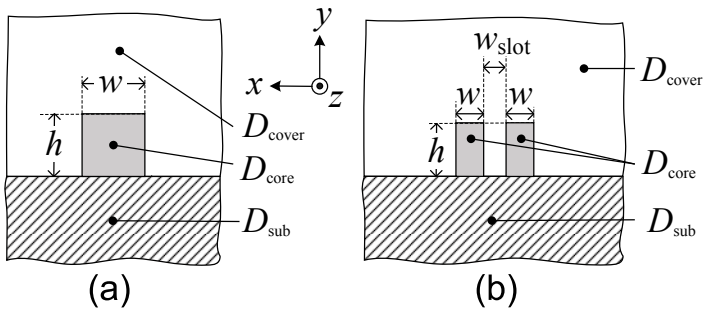

Fig. 1. Waveguide cross-sections (a) Strip waveguide. For core or cover nonlinearity, the nonlinear interaction domain D_{inter} is limited to the core domain ($D_{\text{inter}} = D_{\text{core}}$) or to the cover domain ($D_{\text{inter}} = D_{\text{cover}}$), respectively. (b) Slot waveguide. The nonlinear interaction domain is limited to the cover domain ($D_{\text{inter}} = D_{\text{cover}}$).

interacts with a nonlinear cover material ("cover nonlinearity"). The slot waveguide depicted in Fig. 1(b) enables particularly strong nonlinear interaction of the guided wave with the cover material inside the slot.

For maximum nonlinear interaction in strip or slot waveguides, a set of optimal geometry parameters w and h must exist: Given a nonlinear core and a linear cover, an increase of the waveguide cross section decreases the intensity inside the core and thus weakens the nonlinear interaction, while a decrease of the core size pushes the field more into the linear cover material and again reduces nonlinear effects. If a linear core is embedded into a nonlinear cover, a very small core produces a mode which penetrates the cover too deeply thus reducing the optical intensity in the nonlinear material, while for a large core only a small fraction of light will interact with the nonlinear cover.

Analytical descriptions of third-order nonlinear interaction in optical fibers are given in textbooks [15, 17]. The derivations are adapted to low index-contrast material systems, and it is assumed that the nonlinear susceptibility is constant over the whole cross section. These approximations are excellent for optical fibers and other low-index-contrast systems, but they do not hold for high index-contrast (HIC) waveguides. For example, in the analysis of low index-contrast systems, it is usually assumed that $\nabla \cdot \mathbf{E} = \varepsilon \nabla \cdot \mathbf{D}$, which requires $\nabla \varepsilon \approx 0$ in the entire cross section of the waveguide (see for example Eq. (2.1.18) in [15]). This approximation is not valid for HIC material systems, and the accuracy of standard equations for fibers is questionable when applied to SOI waveguides. We therefore derive a relation for the nonlinear waveguide parameter γ which is adapted to high index-contrast waveguides, where in addition only parts of the cross section are nonlinear. The result is similar to the relations presented in [18]. The mathematical details of the derivation are given in the Appendix.

In the following, the total domain $D_{\text{tot}} = D_{\text{core}} \cup D_{\text{sub}} \cup D_{\text{cover}}$ denotes the total cross section of the waveguide. D_{tot} includes a domain which is filled with the nonlinear interaction material and which is referred to as D_{inter}. The quantity n_{inter} denotes the linear refractive index of the nonlinear material in this interaction domain D_{inter}. For the case of core nonlinearity we have $D_{\text{inter}} = D_{\text{core}}$, $n_{\text{inter}} = n_{\text{core}}$, and for cover nonlinearity $D_{\text{inter}} = D_{\text{cover}}$, $n_{\text{inter}} = n_{\text{cover}}$ has to be used, see Fig. 1. We further approximate the third-order nonlinear susceptibility tensor $\underline{\widetilde{\chi}}^{(3)}$ by a scalar $\widetilde{\chi}^{(3)}$ which is constant within D_{inter}. A simple relationship of the form $\gamma \propto \widetilde{\chi}^{(3)} \Big/ \left(n_{\text{inter}}^2 A_{\text{eff}}\right)$ can then be derived for the nonlinear waveguide parameter γ, see Eq. (16). Denoting the electric and magnetic field vectors of waveguide mode μ by $\mathscr{E}_\mu(x,y)$ and $\mathscr{H}_\mu(x,y)$,

#81030 - $15.00 USD Received 14 Mar 2007; revised 25 Apr 2007; accepted 27 Apr 2007; published 1 May 2007

respectively, the effective area A_{eff} for third-order nonlinear interaction is given by (see Eq. (15) in the Appendix)

$$A_{\text{eff}} = \frac{Z_0^2}{n_{\text{inter}}^2} \frac{\left| \iint_{D_{\text{tot}}} \text{Re}\left\{ \mathscr{E}_\mu(x,y) \times \mathscr{H}_\mu^\star(x,y) \right\} \cdot \mathbf{e}_z \, \text{d}x \, \text{d}y \right|^2}{\iint_{D_{\text{inter}}} \left| \mathscr{E}_\mu(x,y) \right|^4 \text{d}x \, \text{d}y}. \tag{1}$$

$Z_0 = \sqrt{\mu_0/\varepsilon_0} = 377\,\Omega$ is the free-space wave impedance, and $\mathbf{e}_z$ is the unit vector pointing in positive z-direction. For low-index contrast material systems with homogeneous nonlinearity, Eq. (1), (15) reduces to the usual definition of an effective area [15, Eq. (2.3.29)] as is shown in Eq. (17) of the Appendix.

The modal fields $\mathscr{E}_\mu(x,y)$ and $\mathscr{H}_\mu(x,y)$ are classified by the terms TE and TM. TE refers to a waveguide mode with a dominant electric field component in x-direction (parallel to the substrate plane), whereas the dominant electric field component of a TM mode is directed parallel to the y-axis (perpendicular to the substrate plane).

3. Waveguide optimization method

To evaluate the integrals in Eq. (1), both the electric and the magnetic fields of the fundamental waveguide modes are calculated using a commercially available vectorial finite-element mode solver [19]. For core (cover) nonlinearity, the computational domain extends from $-1.5\,\mu$m to $+1.5\,\mu$m ($-2\,\mu$m to $+2\,\mu$m) in the x-direction, and from $-1\,\mu$m to $+2\,\mu$m ($-1.5\,\mu$m to $+2.5\,\mu$m) in the y-direction, terminated by perfectly matched layers of $0.4\,\mu$m thickness in all directions. To improve accuracy, second-order finite elements are used. The size of the finite elements outside the core region is $\Delta x \approx \Delta y \approx 40\,$nm, whereas the silicon strips and the gaps are each divided into at least 10 elements both in the x- and in the y-direction. To better resolve the discontinuities of the normal electric field components, two layers of 2 nm wide finite elements are placed on each side of each dielectric interface. For the structures operated in TM polarization, the fields are evaluated and stored on a rectangular grid with step size $\Delta x_{\text{store}} \approx 5\,$nm in the x-direction and $\Delta y_{\text{store}} \approx 2\,$nm in the y-direction. For TE polarization, the values $\Delta x_{\text{store}} \approx 2\,$nm in x-direction and $\Delta y_{\text{store}} \approx 5\,$nm in y-direction are chosen. The exact step sizes of the grids are matched to hit the dielectric boundaries.

For optimization, the waveguide parameters w and h are alternately scanned in a certain range. The resulting values for A_{eff} are slightly scattered due to numerical inaccuracies. Therefore, a fourth-order polynomial is fitted to the data points, and the local minimum of the polynomial is taken as a starting point for the next scan. The iteration is stopped when the geometrical parameters repeatedly change by less than 0.5 nm between subsequent iterations.

4. Optimal strip and slot waveguides

Third-order nonlinear interaction is maximized for five different cases: Core nonlinearities in strip waveguides for both TE- and TM-polarization, cover nonlinearities in strip waveguides for both polarizations, and cover nonlinearities in TE-operated slot waveguides. For the exploitation of core (cover) nonlinearities, different values of $n_{\text{cover}} \in \{1.0, 1.1, \ldots 2.5\}$ ($n_{\text{cover}} \in \{1.0, 1.1, \ldots 3.0\}$) are considered.

4.1. Strip waveguides and core nonlinearity

For the case of *core nonlinearity*, silicon is used as nonlinear interaction material. Silicon is of point group $m3m$. If Kleinman symmetry is assumed, the susceptibility tensor has two independent elements, $\widetilde{\chi}^{(3)}_{1111} = \widetilde{\chi}^{(3)}_{2222} = \widetilde{\chi}^{(3)}_{3333}$ and $\widetilde{\chi}^{(3)}_{1122} = \widetilde{\chi}^{(3)}_{1212} = \widetilde{\chi}^{(3)}_{1221} = \widetilde{\chi}^{(3)}_{2211} = \cdots = \widetilde{\chi}^{(3)}_{1133} = \cdots = \widetilde{\chi}^{(3)}_{2233} = \ldots$, where the indices 1, 2 and 3 refer to the crystallographic [100], [010] and

#81030 - $15.00 USD Received 14 Mar 2007; revised 25 Apr 2007; accepted 27 Apr 2007; published 1 May 2007

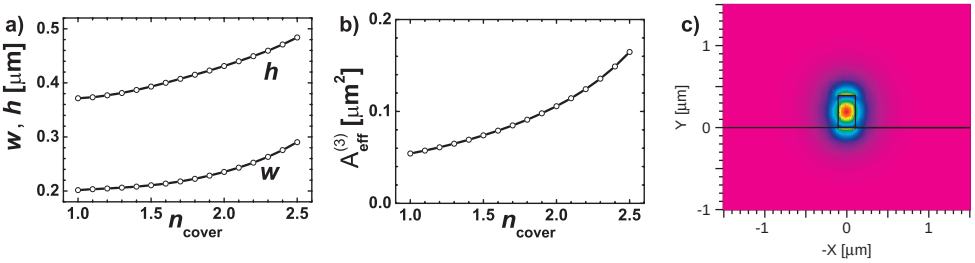

Fig. 2. TM-operated strip waveguide with *core nonlinearity*. Optimized geometrical parameters for a minimum effective area A_{eff} (a) Optimal strip width w and height h as a function of the refractive index n_{cover} of the linear cover material (b) Minimized effective area A_{eff} of nonlinear interaction. (c) Dominant component ($\mathscr{E}_{\mu y}$) of the electric modal field for $n_{\text{cover}} = 1.5$

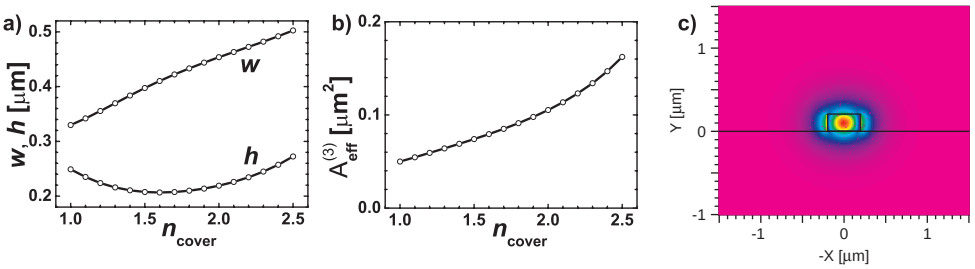

Fig. 3. TE-operated strip waveguide with *core nonlinearity*. Optimized geometrical parameters for a minimum effective area A_{eff} (a) Optimal strip width w and height h as a function of the refractive index n_{cover} of the linear cover material (b) Optimized effective area A_{eff} of nonlinear interaction (c) Dominant component ($\mathscr{E}_{\mu x}$) of the electric modal field for $n_{\text{cover}} = 1.5$

[001] directions. For an isotropic nonlinearity, $\widetilde{\chi}^{(3)}_{1122}/\widetilde{\chi}^{(3)}_{1111} = 1/3$, but for silicon a larger ratio $\widetilde{\chi}^{(3)}_{1122}/\widetilde{\chi}^{(3)}_{1111} = 0.48 \pm 0.03$ has been measured [20]. The assumption of an anisotropic nonlinearity is thus not valid in the strict sense and implies that the components of the nonlinear polarization vector that are not oriented parallel to the exciting electric field vector are neglected. However, the error in calculating the nonlinear waveguide parameter γ is negligible: The TM (TE) mode fields have a dominant $\mathscr{E}_{\mu y}$-component ($\mathscr{E}_{\mu x}$-component), resulting, e.g., in an inaccurate x-component (y-component) of the nonlinear polarization. To calculate the overlap integral in Eq. (14) these components are weighted with the weak $\mathscr{E}_{\mu x}$-component ($\mathscr{E}_{\mu y}$-component) for TM (TE). The overall error is thus very small compared to the contributions of the nonlinear polarization's y-component (x-component). The error in γ would increase, if the interaction between modes of orthogonal polarizations was of interest: The nonlinear polarization generated by a TM (TE) mode is then projected onto a TE (TM) mode field. A small, but inaccurate x-component (y-component) of the nonlinear polarization is thus weighted with the dominant component $\mathscr{E}_{\mu x}$-component ($\mathscr{E}_{\mu y}$-component), whereas the large y-component (x-component) of the nonlinear polarization is weighted by the weak $\mathscr{E}_{\mu x}$-component ($\mathscr{E}_{\mu y}$-component). However, from a practical point of view, theses inaccuracies are small compared to the uncertainties in measured nonlinearities of silicon, Table 1.

Figure 2 shows the results for *core nonlinearity* in a TM-operated strip waveguide. The dominant electric field component ($\mathscr{E}_{\mu y}$) is discontinuous at the horizontal dielectric interfaces with

#81030 - $15.00 USD Received 14 Mar 2007; revised 25 Apr 2007; accepted 27 Apr 2007; published 1 May 2007

a strong field enhancement in the low-index material. Therefore the optimal cross sectional shape of the waveguide core must be narrow and high. This is confirmed by the results of the optimization. It can further be seen that a high index contrast between the core and the cover material always allows for higher field confinement and stronger nonlinear interaction within the core. Effective nonlinear interaction areas as small as $A_{\text{eff}} = 0.054\,\mu\text{m}^2$ can be obtained for $n_{\text{cover}} = 1.0$.

Figure 3 shows the results for *core nonlinearity* in a TE-operated strip waveguide. Using analogous arguments as for the TM case, the optimal cross section of the waveguide core must now be wide and flat. Again, a high index contrast between the core and the cover material always allows for higher field confinement and stronger nonlinear interaction within the core. For low values of n_{cover}, the minimal effective area of nonlinear interaction is slightly smaller for TE polarization than it was TM — for $n_{\text{cover}} = 1.0$ we now find $A_{\text{eff}} = 0.050\,\mu\text{m}^2$. TE-operated strip waveguides with silica cover ($n_{\text{cover}} = 1.44$) and with nearly optimal width $w = 400\,\text{nm}$ and height $h = 200\,\text{nm}$ have previously been used in experiments [4, 21].

4.2. Strip waveguides and cover nonlinearity

The results for *cover nonlinearity* in TM-operated strip waveguides are shown in Fig. 4. The dominant electric field component ($\mathscr{E}_{\mu y}$) is discontinuous at horizontal dielectric interfaces with a strong field enhancement in the nonlinear low-index material. Under these circumstances, the

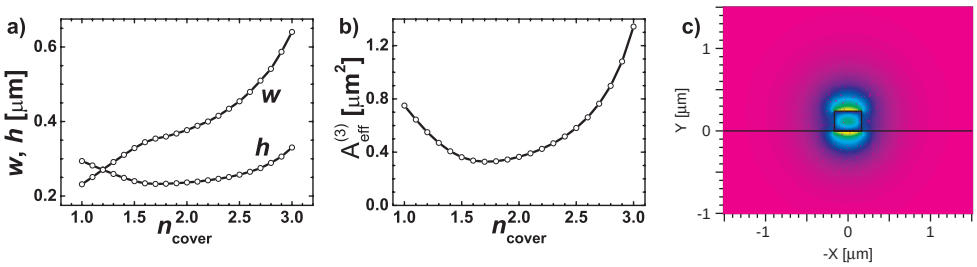

Fig. 4. TM-operated strip waveguide with *cover nonlinearity*. Optimized geometrical parameters for a minimum effective area A_{eff} (a) Optimal strip width w and height h as a function of the linear refractive index n_{cover} of the nonlinear cover material (b) Minimized effective area A_{eff} of nonlinear interaction (c) Dominant component ($\mathscr{E}_{\mu y}$) of the electric modal field for $n_{\text{cover}} = 1.5$

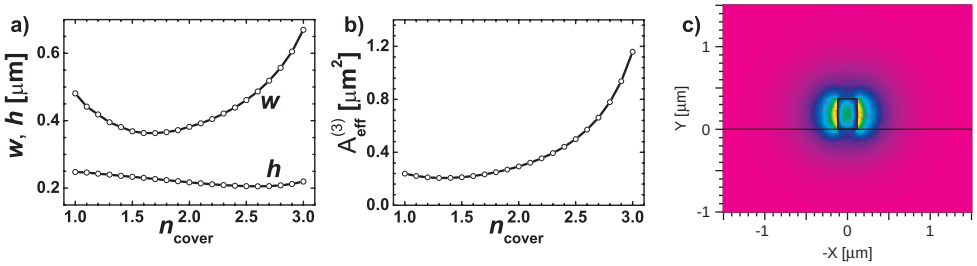

Fig. 5. TE-operated strip waveguide with *cover nonlinearity*. Optimized geometrical parameters for a minimum effective area A_{eff} (a) Optimal strip width w and height h as a function of the linear refractive index n_{cover} of the nonlinear cover material (b) Minimized effective area A_{eff} of nonlinear interaction (c) Dominant component ($\mathscr{E}_{\mu x}$) of the electric modal field for $n_{\text{cover}} = 1.5$

#81030 - $15.00 USD Received 14 Mar 2007; revised 25 Apr 2007; accepted 27 Apr 2007; published 1 May 2007

optimal cross sectional shape of the waveguide is rather wide and flat except for very low refractive indices of the cladding material. It is further found that there is an optimal refractive index $n_{\text{cover}} \approx 1.7$ for which A_{eff} assumes a minimal value of $0.33\,\mu\text{m}^2$. For lower indices, too big a fraction of the electromagnetic field has to be guided within the waveguide core to prevent leakage into the substrate. This part of the field does not contribute to the nonlinear interaction, which makes the effective area bigger. For higher refractive indices, the field enhancement at the dielectric interface decreases, which reduces the nonlinear interaction with the cover material.

In the case of a TE-operated strip waveguide with *cover nonlinearity*, discontinuous field enhancement can be exploited at both sidewalls. This results in smaller effective nonlinear interaction areas as can be seen from Fig. 5. The minimum of A_{eff} now shifts to $n_{\text{cover}} \approx 1.3$ and amounts to roughly $0.24\,\mu\text{m}^2$.

4.3. *Slot waveguides and cover nonlinearity*

For a slot waveguide, most of the light is confined to the slot area, and reducing the slot width w_{slot} increases the intensity in the nonlinear material. Within the range of technologically feasible slot widths, the effective nonlinear interaction area A_{eff} therefore always decreases with w_{slot} and no optimal value for w_{slot} can be found. For the design of slot waveguides, the minimum slot width will be dictated by technological issues, e.g. the maximum aspect ratio that the fabrication process can achieve, or the difficulty of filling a narrow slot with nonlinear inter-

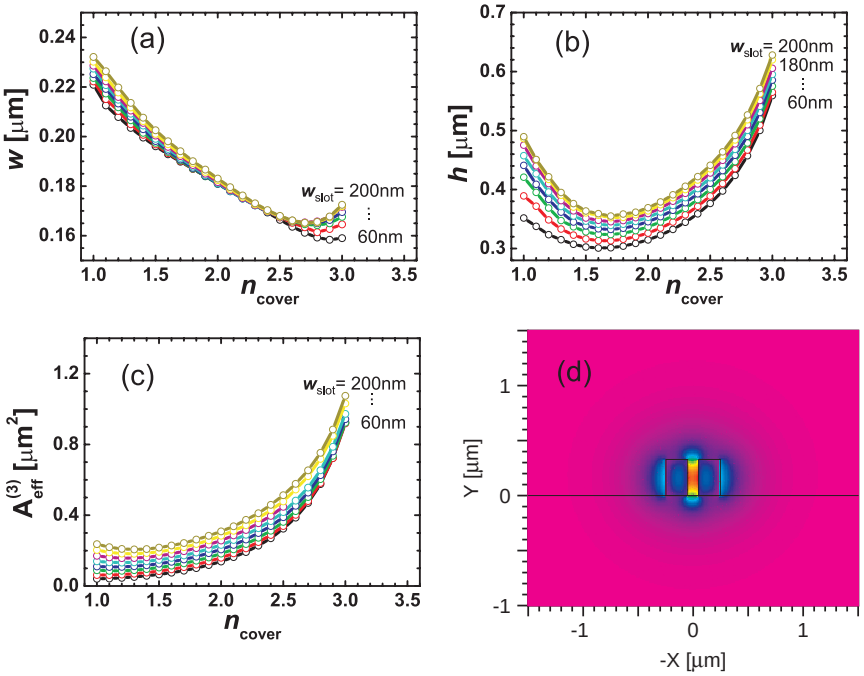

Fig. 6. TE-operated slot waveguide with *cover nonlinearity*. Optimized geometrical parameters for a minimum effective area A_{eff} (a) Optimal strip width w as a function of the linear refractive index n_{cover} of the nonlinear cover material for various slot widths $w_{\text{slot}} \in \{60\,\text{nm}, 80\,\text{nm}, \ldots, 200\,\text{nm}\}$ (b) Optimal strip height h (c) Minimized effective area A_{eff} for nonlinear interaction (d) Dominant component ($\mathscr{E}_{\mu x}$) of the electric modal field for $n_{\text{cover}} = 1.5$ and $w_{\text{slot}} = 100\,\text{nm}$. Click for an animation of $\mathscr{E}_{\mu x}$ for $w_{\text{slot}} = 100\,\text{nm}$ and increasing n_{cover} (file size 700kB).

#81030 - $15.00 USD Received 14 Mar 2007; revised 25 Apr 2007; accepted 27 Apr 2007; published 1 May 2007

action material. Therefore $w_{\mathrm{slot}} \in \{60\,\mathrm{nm},\ 80\,\mathrm{nm} \ldots\ 200\,\mathrm{nm}\}$ is fixed during the optimization procedure.

Figure 6 shows the optimal parameters as a function of the refractive index n_{cover} of the nonlinear cover material with the slot width w_{slot} as a parameter. The width w of the individual strips mainly depends on n_{cover}, whereas the optimal height h shows substantial variations with both n_{cover} and w_{slot}. For $w_{\mathrm{slot}} \geq 100\,\mathrm{nm}$, there is again an optimal refractive index n_{cover} for which A_{eff} is minimum. The existence of this minimum can be explained physically: For larger refractive indices, the discontinuity-induced field enhancement at the dielectric interfaces decreases. For lower refractive indices, the increase in field enhancement is over-compensated by the fact that a minimum fraction of the electromagnetic field has to be guided in the high-index core material to prevent leakage into the substrate. This fraction of the field does not contribute to the nonlinear interaction and thus increases A_{eff}. For $w_{\mathrm{slot}} < 100\,\mathrm{nm}$, the guidance of the fundamental mode is always strong enough to prevent it from leaking into the substrate, and A_{eff} decreases monotonically as n_{cover} decreases.

Similar arguments hold for explaining the behaviour of the optimal height: For decreasing refractive indices, the height increases in the case of $w_{\mathrm{slot}} \geq 120\,\mathrm{nm}$ to prevent leakage into the substrate. For $w_{\mathrm{slot}} < 120\,\mathrm{nm}$ this does not seem to be crucial, and the optimal height even decreases slightly for small values of n_{cover}. Using slot waveguides with technologically feasible gap widths of 100 nm results in effective nonlinear interaction areas as small as $A_{\mathrm{eff}} = 0.086\,\mu\mathrm{m}^2$ or $A_{\mathrm{eff}} = 0.105\,\mu\mathrm{m}^2$ for $n_{\mathrm{cover}} = 1.2$ or $n_{\mathrm{cover}} = 1.5$, respectively.

5. Nonlinear parameters for different materials

The previous analysis shows that outstandingly small effective areas A_{eff} can be obtained in SOI-based waveguides, and it can be expected that, depending on the properties of the employed materials, highly nonlinear integrated waveguides can be realized. We will now estimate the nonlinear parameter $\mathrm{Re}\{\gamma\}$ for different interaction materials.

Nonlinear properties of optical materials are commonly described by a nonlinear refractive index which depends on the intensity I of an optical wave, $n = n_0 + n_2 I$, and by a corresponding intensity-dependent power absorption coefficient $\alpha = \alpha_0 + \alpha_2 I$. The nonlinear refractive index n_2 and the TPA coefficient α_2 are linked to the scalar third-order nonlinear optical susceptibility $\widetilde{\chi}^{(3)}$ by [15, Eq. (2.3.13)]

$$n_2 = \frac{3 Z_0 \,\mathrm{Re}\left\{\widetilde{\chi}^{(3)}\right\}}{4 n_0^2}, \tag{2}$$

$$\alpha_2 = -\frac{3 k_0 Z_0 \,\mathrm{Im}\left\{\widetilde{\chi}^{(3)}\right\}}{2 n_0^2}. \tag{3}$$

TPA leads to a strong decay of optical power along the direction of propagation and can therefore severely impair nonlinear parametric effects such as SPM, XPM and FWM [22]. A measure of this impairment is the TPA figure of merit $\mathrm{FOM}_{\mathrm{TPA}}$, which is the nonlinear phase shift related to the associated intensity change and may be expressed through the nonlinear parameter γ, see Eq. (16),

$$\mathrm{FOM}_{\mathrm{TPA}} = -\frac{1}{2\pi}\,\frac{\mathrm{Re}\{\gamma\}}{2\,\mathrm{Im}\{\gamma\}} = \frac{n_2}{\alpha_2 \lambda}. \tag{4}$$

An optical power P_0 launched into a waveguide of length L would account for a nonlinear phase shift of $\Delta\phi_{\mathrm{nl}} = \mathrm{Re}\{\gamma\} P_0 L$ in the absence of loss. TPA reduces the power along the propagation length, $P(L) = P_0/(1 + \frac{\Delta\phi_{\mathrm{nl}}}{2\pi}\mathrm{FOM}_{\mathrm{TPA}})$, thereby reducing the nonlinear phase shift. To achieve

#81030 - $15.00 USD Received 14 Mar 2007; revised 25 Apr 2007; accepted 27 Apr 2007; published 1 May 2007

Material	$\mathrm{Re}\{\gamma\}/(\mathrm{W\,m})^{-1}$ $\mathrm{TM_{strip}}$	$\mathrm{TE_{strip}}$	λ/nm	n_0	$n_2/(\mathrm{m^2/W})$	$\mathrm{FOM_{TPA}}$	Ref.
Silicon	449	487	1550	3.48	6×10^{-18}	0.86	[9]
	336	365	1540	3.48	4.5×10^{-18}	0.37	[24]
	322	349	1540	3.48	4.3×10^{-18}	0.32	[24]
	1080	1180	1550	3.48	14.5×10^{-18}	1.56	[10]
	374	406	1550	3.48	5×10^{-18}		[11]

Table 1. Core nonlinearity. Calculated maximum nonlinearity parameters $\mathrm{Re}\{\gamma\}\propto 1/A_{\mathrm{eff}}$ for optimized strip waveguides with a nonlinear silicon core and a linear air cladding $n_{\mathrm{cover}}=1$, operated in TM or TE polarization. The calculation is based on data for silicon at the specified wavelengths: Linear refractive index n_0, nonlinearity coefficient n_2 and TPA figure of merit $\mathrm{FOM_{TPA}}$ were taken from the references listed in the last column. — The resulting nonlinear parameters $\mathrm{Re}\{\gamma\}\approx 400/(\mathrm{W\,m})$ are remarkably large. However, the material suffers from non-negligible two-photon absorption leading to a figure of merit $\mathrm{FOM_{TPA}}\approx 0.3\ldots0.9$.

SPM-induced nonlinear phase-shifts $\Delta\phi_{\mathrm{nl}}>2\pi$ ($\Delta\phi_{\mathrm{nl}}>\pi$), the interaction material should satisfy $\mathrm{FOM_{TPA}}>1$ ($\mathrm{FOM_{TPA}}>0.5$) [23].

Tables 1 and 2 list the calculated optimum nonlinear parameters $\mathrm{Re}\{\gamma\}$ as defined in Eq. (16) for various nonlinear core and cover materials, polarizations and structures. In both tables these calculations are based on material data at the specified wavelengths, namely on the linear refractive index n_0 and on the nonlinearity coefficient n_2. In addition, the TPA figure of merit $\mathrm{FOM_{TPA}}$ is specified. All material data were taken from the references listed in the last column of both tables. For some materials, no $\mathrm{FOM_{TPA}}$ data at 1550 nm could be found. Some nonlinearity data were only available from third-harmonic generation experiments, which is indicated in Table 2 by an asterisk$^{\star)}$ after the wavelength. In these cases the calculated maximum nonlinear parameter $\mathrm{Re}\{\gamma\}$ might be inaccurate, but should still reflect the correct order of magnitude.

Table 1 refers to the case of *core nonlinearity* with silicon as the nonlinear core material. Reported nonlinearity coefficients n_2 for silicon range from $4.3\times10^{-18}\,\mathrm{m^2/W}$ to $14.5\times10^{-18}\,\mathrm{m^2/W}$. The nonlinear parameters $\mathrm{Re}\{\gamma\}$ have been calculated for optimized strip waveguides with air as a cover material ($n_{\mathrm{cover}}=1.0$). Optimal strip widths and heights for TM-polarization, ("$\mathrm{TM_{strip}}$", $A_{\mathrm{eff}}=0.054\,\mu\mathrm{m^2}$) and for TE-polarization ("$\mathrm{TE_{strip}}$", $A_{\mathrm{eff}}=0.050\,\mu\mathrm{m^2}$) are obtained from Figs. 3 and 2. Depending on the value of n_2, the resulting nonlinear waveguide parameters range from $322/(\mathrm{W\,m})$ to $1180/(\mathrm{W\,m})$. TPA figures of merit around 1 indicate that parametric effects such as SPM, XPM and FWM will usually be impaired by TPA.

Table 2 refers to the case of *cover nonlinearity*. The interaction material must have a linear refractive index $n_{\mathrm{inter}}=n_0$ smaller than the index of silicon and provide low linear and nonlinear absorption in the desired wavelength range. There is a vast choice of such materials, and we have concentrated on the most prominent ones for which reliable data on nonlinear parameters could be obtained. These materials are subdivided into three groups: Inorganic materials (glasses), organic materials (polymers) and nanocomposites (e.g. artificial nanocrystals).

For each material, we have estimated the nonlinear parameter $\mathrm{Re}\{\gamma\}$ for three different cases: A TM-operated strip waveguide ("$\mathrm{TM_{strip}}$"), a TE-operated strip waveguide ("$\mathrm{TE_{strip}}$"), and a TE-operated slot waveguide with $w_{\mathrm{slot}}=100\,\mathrm{nm}$ ("$\mathrm{TE_{slot}}$"). All these waveguides have geometries optimized for the respective cover material, see Figs. 4, 5 and 6. The nonlinear parameter $\mathrm{Re}\{\gamma\}$ denotes the contribution of the nonlinear cover material only — the contribution of the

#81030 - $15.00 USD Received 14 Mar 2007; revised 25 Apr 2007; accepted 27 Apr 2007; published 1 May 2007

Material	$\mathrm{Re}\{\gamma\}/(\mathrm{W\,m})^{-1}$ TM$_{\mathrm{strip}}$	TE$_{\mathrm{strip}}$	TE$_{\mathrm{slot}}$	λ / nm	n_0	$n_2/(\mathrm{m}^2/\mathrm{W})$	FOM$_{\mathrm{TPA}}$	Ref.
Inorganic materials								
Pure silica glass	0.3	0.5	1.0	1550	1.45	2.48×10^{-20}	$\gg10$	[15]
Lead silicate glass								
Schott SF59	8.0	11	17	1060	1.91	6.8×10^{-19}		[25]
Bismite glass	3.5	4.4	6.9	1550	2.02	3.2×10^{-19}		[26]
Tellurite glass								
Li_2O-TiO_2-TeO_2	6.2	7.5	11	1900$^{\star)}$	2.2	6.53×10^{-19}		[27]
Chalcogenide glass								
$As_{24}S_{38}Se_{38}$	74	86	120	1600	2.45	1.0×10^{-17}		[28]
$As_{39}Se_{61}$	71	82	105	1500	2.81	1.6×10^{-17}	3.8	[29]
$As_{40}Se_{60}$	102	117	151	1500	2.81	2.3×10^{-17}	11	[29]
Organic materials								
PDA	54	92	186	1319	$\sim$1.5	4.8×10^{-18}	1.5	[30, 31]
PTA	22	38	78	1907$^{\star)}$	1.5	2×10^{-18}		[23]
TEE	17	29	58	1907$^{\star)}$	1.5	1.5×10^{-18}		[32]
PSTF66	31	54	109	1550	1.5	2.8×10^{-18}	0.22	[33, 34]
DANS	94	149	293	1319	1.57	8×10^{-18}	7.6	[35]
PTS (PDA)	2720	3820	6950	1600	$\sim$1.7	2.2×10^{-16}	>27	[36, 37]
Nanocomposites								
Si nanocrystals	22800	33100	61600	813	1.66	1.86×10^{-15}	5.6	[38]
	1120	1910	4000	1500	1.5	$\sim10^{-16}$		[7]

$^{\star)}$ Third-order nonlinearity obtained by third-harmonic generation

Table 2. Cover nonlinearity. Calculated maximum nonlinearity parameters $\mathrm{Re}\{\gamma\} \propto 1/A_{\mathrm{eff}}$ for optimized strip and slot waveguides with a linear silicon core and various nonlinear cover materials, operated in TM or TE polarization. The calculation is based on cover material data at the specified wavelengths: Linear refractive index n_0, nonlinearity coefficient n_2 and TPA figure of merit FOM$_{\mathrm{TPA}}$ were taken from the references listed in the last column. Three material groups are considered: Inorganic materials like glasses, organic substances, and nanocomposites. — Most remarkable are the large nonlinear parameters $\mathrm{Re}\{\gamma\} \approx (70\ldots150)/(\mathrm{W\,m})$ and $\mathrm{Re}\{\gamma\} \approx 300/(\mathrm{W\,m})$ for chalcogenide glasses and for the side-chain polymer DANS, respectively, and the record value of $\mathrm{Re}\{\gamma\} \approx 7000/(\mathrm{W\,m})$ for the single-crystalline organic material PTS, a number which is 1000 times larger than for a higly nonlinear bismite glass. These material groups have also very good TPA figures of merit in the order of FOM$_{\mathrm{TPA}} \approx 4\ldots27$.

silicon core is not taken into account, and the values for $\mathrm{Re}\{\gamma\}$ as listed in Tab. 2 are to be understood as lower bounds for the nonlinear parameter. While the waveguides discussed in Tab. 1 are designed with a nonlinear core material, the structures in Tab. 2 have been optimized for cover nonlinearity; the contribution of the silicon core is in this case significantly smaller than could be inferred from Tab. 1.

The first group of nonlinear cover materials comprises different glasses. Silica glass (SiO_2) is not a typical nonlinear material, but for comparison, we have calculated the corresponding nonlinear parameters. We note that the resulting values $\mathrm{Re}\{\gamma\} \leqslant 1.0/(\mathrm{W\,m})$ are in the same order of magnitude as the nonlinear parameters obtained for modern highly-nonlinear fibers based on lead silicate glasses, $\mathrm{Re}\{\gamma\} = 1.86/(\mathrm{W\,m})$ [16]. Lead silicate glasses, bismite glasses, tellurite glasses and chalcogenide glasses feature high linear and high nonlinear refractive indices n_0 and

#81030 - $15.00 USD Received 14 Mar 2007; revised 25 Apr 2007; accepted 27 Apr 2007; published 1 May 2007

n_2. The high linear indices considerably reduce the discontinuity-induced field enhancement at the dielectric interfaces, so that A_{eff} increases and the nonlinear parameter decreases. For the slot waveguide, we find $A_{\text{eff}} = 0.62\,\mu\text{m}^2$ given $n_{\text{cover}} = 2.81$, which is roughly a factor of 6 bigger than the value of $A_{\text{eff}} = 0.104\,\mu\text{m}^2$ for $n_{\text{cover}} = 1.5$. Still, the nonlinear parameters $\text{Re}\{\gamma\}$ are nearly two orders of magnitude larger than for state-of-the-art highly nonlinear fibers [16].

The second group of nonlinear materials comprises nonlinear organic materials. Nonlinearities in these materials can either arise from the polymer backbone, or from chromophore units embedded in the host matrix or laterally attached to the backbone. For the conjugated polymers PDA (polydiacetylene), PTA (polytriactelyene) and TEE (tetraethynylethene), nonlinearities are roughly two orders of magnitude stronger than for SiO_2. Please note that the nonlinear refractive indices for PTA and TEE have been measured via third-harmonic generation (THG) at a pump wavelength of 1900 nm, and the results cannot offhand be applied to SPM at 1550 nm. The order of magnitude might be correct, though. The organic dye functionalized main-chain polymer PSTF66 exhibits large nonlinear losses, whereas the side chain polymer DANS (4-dialkyamino-4'nitro-stilbene) exhibits TPA figures of merit that are suitable for devices based on nonlinear phase shifts. For single-crystalline poly(p-toluene sulphonate) (PTS) polydiacetylene, nonlinear refraction is even four orders of magnitude stronger than for SiO_2, and nonlinear parameters $\text{Re}\{\gamma\}$ in the order of $6950/(\text{W m})$ can be expected for slot waveguides without severe impairment by TPA. For strip waveguides, $\text{Re}\{\gamma\}$ reduces by roughly 50 %, but is still about $3820/(\text{W m})$. Using single-crystal PTS as a nonlinear interaction material around a prestructured silicon waveguide core might also solve the problem of poor processability of single crystal PTS.

Lastly, we consider the case where the slot waveguide is filled with artificial silicon nanocrystals. At $\lambda = 813$ nm this nanocomposite material exhibits huge nonlinearities (about five order of magnitudes stronger than in SiO_2) without impairment by TPA. It is questionable which nonlinearities can be obtained at 1550 nm, but even if only values of $n_0 = 1.50$ and $n_2 = 10^{-16}\,\text{m}^2/\text{W}$ are assumed, as has been done by other authors [7], large nonlinear parameters $\text{Re}\{\gamma\}$ up to $4000/(\text{W m})$ can be expected.

6. Discussion

For state-of-the-art highly nonlinear fibers, the highest nonlinear parameters $\text{Re}\{\gamma\}$ are in the order of $2/(\text{W m})$ [16]. According to our estimations, a nonlinear parameter more than three orders of magnitude larger can be expected for SOI-based strip and slot waveguides covered with appropriate nonlinear interaction materials. Approximately one order of magnitude is gained from the strong confinement of the electromagnetic field. Because waveguides with cover nonlinearities allow to choose from a broad spectrum of interaction materials, the extremely nonlinear PTS-system can be chosen, which leads to an additional improvement of approximately two orders of magnitude compared to lead silicate glass.

Highly-nonlinear integrated strip and slot waveguides are viable for on-chip all-optical signal processing as shall be illustrated by estimating the lengths required for a passive SPM/XPM-based switch and a passive wavelength converter based on FWM.

The nonlinear phase shift $\Delta\phi_{\text{nl}}$ experienced by an optical signal through SPM or XPM in a lossless waveguide is proportional to the optical power P and the interaction length L, $\Delta\phi_{\text{nl}} = \text{Re}\{\gamma\}PL$ or $\Delta\phi_{\text{nl}} = 2\,\text{Re}\{\gamma\}PL$, respectively. For many nonlinear signal processing schemes, a nonlinear phase shift of $\Delta\phi_{\text{nl}} = \pi$ is required. If an optical peak power of $P = 100$ mW and a slot waveguide with a nonlinear waveguide parameter of $\text{Re}\{\gamma\} = 6950/(\text{W m})$ are assumed, a nonlinear phase shift of π requires a slot waveguide with a length of $L = 4.5$ mm or $L = 2.3$ mm, respectively. For $\text{Re}\{\gamma\} = 3820/(\text{W m})$ as calculated for a TE-operated strip waveguide, the length increases to $L = 8.2$ mm or $L = 4.1$ mm, again for SPM or XPM, respectively.

#81030 - $15.00 USD Received 14 Mar 2007; revised 25 Apr 2007; accepted 27 Apr 2007; published 1 May 2007

Neglecting waveguide loss and pump depletion, and assuming phase matching, the conversion efficiency for degenerate FWM is given by $\eta_{\mathrm{FWM}} = \left(\mathrm{Re}\{\gamma\} P_{\mathrm{pmp}} L\right)^2$, where P_{pmp} denotes the pump power [15]. Assuming again a slot waveguide with $\mathrm{Re}\{\gamma\} = 6950/(\mathrm{W\,m})$ and $P_{\mathrm{pmp}} = 100\,\mathrm{mW}$, a conversion efficiency of 100 % can be obtained for an estimated waveguide length of $L = 1.4\,\mathrm{mm}$. For a TE-operated strip waveguide with $\mathrm{Re}\{\gamma\} = 3820/(\mathrm{W\,m})$, this length increases to $L = 2.6\,\mathrm{mm}$.

These results indicate that broadband, i. e., nonresonant ultrafast all-optical signal processing is feasible with compact mm-long integrated devices based on highly nonlinear slot and strip waveguides. We note that in all cases the assumed power levels are far too low to induce saturation of the nonlinear phase shift due to a Kerr-induced decrease of the discontinuity-induced field enhancement [39]. As with all nonlinear switching processes, the switching power and/or the interaction length can be considerably reduced at the expense of bandwidth by using resonant structures [7]. Compared to signal processing schemes based on active integrated devices, e.g., semiconductor optical amplifiers, passive schemes need higher power levels. However, passive Kerr-based devices are ultra-fast, do not exhibit pattern effects, and do not require active cooling.

7. Summary

SOI-based nonlinear strip and slot waveguides are well suited for ultrafast all-optical signal processing if an appropriate cover material is applied. A newly introduced effective area A_{eff} for third-order nonlinear interaction in high index-contrast waveguides with nonlinear constituents serves as a basis for the optimization of different SOI-based waveguide structures with respect to a maximum nonlinearity parameter γ. We provide universal optimal design parameters for strip and slot waveguides covered with different nonlinear interaction materials, and we calculate the resulting maximum nonlinear parameter γ. It is found that γ can be more than three orders of magnitude larger compared with state-of-the-art highly nonlinear fibers. Estimating the waveguide lengths for different nonlinear signal processing schemes, we infer that nonresonant ultrafast nonlinear signal processing is possible with mm-scale integrated SOI-based devices.

Acknowledgement

This work was supported by the Center for Functional Nanostructures (CFN) of the Deutsche Forschungsgemeinschaft (DFG) within projects A3.1 and A4.4, and by the European project TRIUMPH (grant IST-027638 STP). We acknowledge fruitful discussions with U. Gubler.

Appendix: Third-order nonlinear interaction in high index-contrast waveguides

In this Appendix we derive the basic nonlinear propagation equation for a nonlinear high-index-contrast waveguide. We start from Maxwell's curl equations for the electric and the magnetic field,

$$\nabla \times \mathbf{H}(\mathbf{r},t) = \frac{\partial \mathbf{D}(\mathbf{r},t)}{\partial t} \tag{5}$$

$$\nabla \times \mathbf{E}(\mathbf{r},t) = -\frac{\partial \mathbf{B}(\mathbf{r},t)}{\partial t}, \tag{6}$$

where $\mathbf{B} = \mu_0\,\mathbf{H}$ and where the electrical displacement $\mathbf{D} = \varepsilon_0 n^2 \mathbf{E} + \mathbf{P}^{(\mathrm{nl})}$ contains the third-order nonlinear polarization $\mathbf{P}^{(\mathrm{nl})}$. Assuming a medium response that is local in space, $\mathbf{P}^{(\mathrm{nl})}$ can be written in tensor notation,

$$\mathbf{P}^{(\mathrm{nl})}(t) = \varepsilon_0 \iiint \underline{\chi}^{(3)}(\tau_1,\tau_2,\tau_3) \vdots \mathbf{E}(t-\tau_1)\mathbf{E}(t-\tau_2)\mathbf{E}(t-\tau_3)\,\mathrm{d}\,\tau_1\,\mathrm{d}\,\tau_2\,\mathrm{d}\,\tau_3, \tag{7}$$

#81030 - $15.00 USD Received 14 Mar 2007; revised 25 Apr 2007; accepted 27 Apr 2007; published 1 May 2007

where $\vdots$ denotes the tensor product; the spatial argument $\mathbf{r}$ was omitted. The optical signal propagating in the μth mode of the waveguide is described in slowly-varying envelope approximation (SVEA) of a carrier signal at frequency ω_c,

$$\mathbf{E}_\mu(\mathbf{r},t) = \mathrm{Re}\left\{ A_\mu(z,t)\frac{\mathscr{E}_\mu(x,y,\omega_c)}{\sqrt{\mathscr{P}_\mu}}\,\mathrm{e}^{\mathrm{j}(\omega_c t-\beta_\mu(\omega_c)z)}\right\}, \tag{8}$$

$$\mathbf{H}_\mu(\mathbf{r},t) = \mathrm{Re}\left\{ A_\mu(z,t)\frac{\mathscr{H}_\mu(x,y,\omega_c)}{\sqrt{\mathscr{P}_\mu}}\,\mathrm{e}^{\mathrm{j}(\omega_c t-\beta_\mu(\omega_c)z)}\right\}. \tag{9}$$

Here, $A_\mu(z,t)$ is the complex envelope, $\mathscr{E}_\mu(x,y,\omega_c)$ and $\mathscr{H}_\mu(x,y,\omega_c)$ denote the vectorial electric and magnetic mode profiles in a transverse plane of the waveguide, $\beta_\mu(\omega_c)$ is the associated propagation constant of the carrier wave, and $\mathscr{P}_\mu$ is used for power normalization of the numerically computed mode fields,

$$\mathscr{P}_\mu = \frac{1}{2}\int_{-\infty}^{\infty}\int_{-\infty}^{\infty}\mathrm{Re}\left\{\mathscr{E}_\mu(x,y,\omega_c)\times\mathscr{H}_\mu^\star(x,y,\omega_c)\right\}\cdot\mathbf{e}_z\,\mathrm{d}x\,\mathrm{d}y. \tag{10}$$

In this definition, $A_\mu(z,t)$ has the dimension $\sqrt{\mathrm{W}}$, and the power of the signal averaged over some optical periods is given by $\left|A_\mu(z,t)\right|^2$. We further need the orthogonality of the transverse mode fields [40],

$$\frac{1}{4}\int_{-\infty}^{\infty}\int_{-\infty}^{\infty}[(\mathscr{E}_\mu\times\mathscr{H}_{\mu'}^\star)+(\mathscr{E}_{\mu'}^\star\times\mathscr{H}_\mu)]\cdot\mathbf{e}_z\,\mathrm{d}x\,\mathrm{d}y = \mathscr{P}_\mu\delta_{\mu,\mu'}, \tag{11}$$

where we have omitted the arguments (x,y,ω_c).

Three approximations are involved in the following analysis: First, we assume that the nonlinear polarization is weak compared to the linear contribution and can therefore be treated as a small perturbation that changes the complex amplitude $A_\mu(z,t)$ during propagation. Second, the SVEA is used, and we assume that the nonlinear response of the medium is instantaneous on the time-scale of the pulse envelope $A_\mu(z,t)$, which allows us to simplify the triple convolution integral in Eq. (7) into a normal tensor product for the mode fields. Third, the dispersion relation of the waveguide is approximated by a second-order Taylor expansion about the carrier frequency ω_c,

$$\beta(\omega) = \beta_\mu + (\omega-\omega_\mathrm{c})\beta_\mu^{(1)} + \frac{1}{2}(\omega-\omega_\mathrm{c})^2\beta_\mu^{(2)}, \tag{12}$$

where $\beta_\mu^{(n)} = \left.\frac{\mathrm{d}^n\beta_\mu}{\mathrm{d}\omega^n}\right|_{\omega=\omega_\mathrm{c}}$. We note that there are no restrictions for the shape of the mode fields, for the refractive index profile of the waveguide or for the spatial distribution of $\underline{\chi}^{(3)}$.

The derivation of the nonlinear propagation equation for a single monochromatic signal involves several algebraic modifications which will be described only briefly. We first insert the nonlinear polarization according to Eq. (7) into the right-hand side of Eq. (5). We then use a mode expansion according to Eq. (8) (Eq. (9)) on the left-hand side of Eq. (6) (Eq. (5)) and apply the identity $\nabla\times(\Phi\mathscr{F}) = \Phi(\nabla\times\mathscr{F})+(\nabla\Phi)\times\mathscr{F}$, where $\Phi = A_\mu(z,t)\,\mathrm{e}^{\mathrm{j}[\omega_c t-\beta(\omega_c)z]}$ represents a scalar function, and $\mathscr{F} = \mathscr{E}_\mu(x,y,\omega_c)/\sqrt{\mathscr{P}_\mu}$ ($\mathscr{F} = \mathscr{H}_\mu(x,y,\omega_c)/\sqrt{\mathscr{P}_\mu}$) is a vector field. The amplitudes associated with the μth mode on the right-hand side are then projected out by taking the scalar product of both sides with $\mathscr{H}_\mu^\star(x,y,\omega_c)$ ($\mathscr{E}_\mu^\star(x,y,\omega_c)$) followed by an integration over the entire cross section. The resulting equations are then added and Eq. (11) is applied. We finally obtain the nonlinear Schrödinger equation,

$$\frac{\partial A_\mu(z,t)}{\partial z}+\beta_\mu^{(1)}\frac{\partial A_\mu(z,t)}{\partial t}-\mathrm{j}\,\frac{1}{2}\beta_\mu^{(2)}\frac{\partial^2 A_\mu(z,t)}{\partial t^2} = -\mathrm{j}\,\gamma\left|A_\mu(z,t)\right|^2 A_\mu(z,t), \tag{13}$$

#81030 - $15.00 USD Received 14 Mar 2007; revised 25 Apr 2007; accepted 27 Apr 2007; published 1 May 2007

where the nonlinear parameter γ is given by

$$\gamma = \frac{3\omega_c \varepsilon_0}{16\,\mathscr{P}_\mu^2} \iint \left[\underline{\widetilde{\chi}}^{(3)}(\omega_c : \omega_c, \omega_c, -\omega_c) \vdots \mathscr{E}_\mu(\omega_c)\,\mathscr{E}_\mu(\omega_c)\,\mathscr{E}_\mu^\star(\omega_c) \right] \cdot \mathscr{E}_\mu^\star(\omega_c)\,\mathrm{d}x\,\mathrm{d}y. \tag{14}$$

The spatial arguments (x,y) have been again omitted. The quantity $\underline{\widetilde{\chi}}^{(3)}$ is the frequency-domain representation of the nonlinear susceptibility tensor.

For many cases of practical interest, only the core or the cover material have a $\chi^{(3)}$-nonlinearity, which is usually isotropic. The third-order nonlinear susceptibility tensor $\underline{\chi}^{(3)}$ can then assumed to be zero outside a nonlinear interaction domain D_{inter} (refractive index n_{inter}), and it is nonzero and constant inside D_{inter}. Further, $\underline{\widetilde{\chi}}^{(3)}$ may be approximated by a scalar $\widetilde{\chi}^{(3)}$, so that $\underline{\widetilde{\chi}}^{(3)} \vdots \mathscr{E}_\mu \mathscr{E}_\mu \mathscr{E}_\mu^\star = \widetilde{\chi}^{(3)} \left|\mathscr{E}_\mu\right|^2 \mathscr{E}_\mu$ holds. To evaluate only the effects of the waveguide geometry, the strength of the nonlinear interaction of the guided modes can then be compared to a hypothetical plane wave in bulk nonlinear material with the same nonlinear susceptibility $\chi^{(3)}$ and the same refractive index as D_{inter}.

This leads to the concept of an effective nonlinear interaction area A_{eff}: In a waveguide with a nonlinear interaction region D_{inter} the cross-sectional power P is transported. Relating P to the effective area A_{eff} leads to an effective intensity $I = P/A_{\text{eff}}$. This intensity I should be attributed to a plane wave which propagates in a homogeneous medium with the same optical properties as seen in D_{inter}. For this effective area we find

$$A_{\text{eff}} = \frac{Z_0^2}{n_{\text{inter}}^2} \frac{\left| \iint_{D_{\text{tot}}} \mathrm{Re}\left\{ \mathscr{E}_\mu(x,y) \times \mathscr{H}_\mu^\star(x,y) \right\} \cdot \mathbf{e}_z \,\mathrm{d}x\,\mathrm{d}y \right|^2}{\iint_{D_{\text{inter}}} \left|\mathscr{E}_\mu(x,y)\right|^4 \mathrm{d}x\,\mathrm{d}y}. \tag{15}$$

The nonlinear waveguide parameter γ then simplifies to the expression

$$\gamma = \frac{3\omega_c \varepsilon_0 Z_0^2}{4 A_{\text{eff}}\, n_{\text{inter}}^2} \widetilde{\chi}^{(3)}. \tag{16}$$

For complex values of $\widetilde{\chi}^{(3)}$the nonlinear parameter γ will be also complex, and parametric $\chi^{(3)}$-processes (e.g. SPM, XPM, FWM) will be impaired by nonparametric processes (e.g. TPA).

For low index-contrast material systems, the approximation $n_{\text{core}} \approx n_{\text{cover}} \approx n_{\text{inter}}$ holds, and the longitudinal field components become negligible. The transverse components of the mode fields $\mathscr{E}_\mu(x,y)$ and $\mathscr{H}_\mu(x,y)$ may then be approximated by a scalar function $F(x,y)$, $\mathscr{E}_\mu(x,y) \approx F(x,y)\,\mathbf{e}_x$, $\mathscr{H}_\mu(x,y) \approx \frac{n_{\text{inter}}}{Z_0} F(x,y)\,\mathbf{e}_y$. If we further assume a homogeneous nonlinearity, then $D_{\text{inter}} = D_{\text{tot}}$, and Eq. (15) can be simplified to

$$A_{\text{eff}} \approx \frac{\left(\iint_{D_{\text{tot}}} |F(x,y)|^2 \,\mathrm{d}x\,\mathrm{d}y \right)^2}{\iint_{D_{\text{tot}}} |F(x,y)|^4 \,\mathrm{d}x\,\mathrm{d}y}. \tag{17}$$

This relation is identical with the usual definition of an effective area A_{eff} [15, Eq. (2.3.29)].

#81030 - $15.00 USD Received 14 Mar 2007; revised 25 Apr 2007; accepted 27 Apr 2007; published 1 May 2007